

Effects of Dipolar Interactions on Linear and Nonlinear Optical Properties of Multichromophore Assemblies: A Case Study

Francesca Terenziani, Olivier Mongin, Claudine Katan, Bharath Kumar Goud Bhatthula, and Mireille Blanchard-Desce*^[a]

In memory of Rüdiger Wortmann

Abstract: Interchromophore interactions in flexible multidipolar structures for nonlinear optics were addressed by a combined experimental and theoretical study on two series of one-, two-, and three-chromophore systems in which identical push–pull chromophores are assembled through covalent and flexible linkers in close proximity. The photophysical and nonlinear optical properties (quadratic hyperpolarizability) of the multichromophore systems were investigated and compared to those of the monomeric chromophores. Multimers have larger dipole moments than their monomeric analogues, that is, the dipolar subchromophores self-orientate within the multimeric structures. This effect was found to depend on the intersubchromophore

distance in a nontrivial manner, which confirms that molecular engineering of such flexible systems is more complex than in completely geometrically controlled systems. Electric-field-induced second-harmonic generation (EFISHG) measurements in solution revealed increased figures of merit as compared to the monomeric analogue. This effect increases with increasing number and polarity of the individual subchromophores in the nanoassembly and increasing spacing between dipolar subchromophores. Experimental results are interpreted by a theoretical model

Keywords: chromophores • fluorescence • nonlinear optics • self-organization • theoretical models


for interacting polar and polarizable chromophores. The properties of multidipolar assemblies are shown to be related to the relative orientation of chromophores, which is imposed by interchromophore interactions. The supramolecular structure is thus a result of self-organization. The proposed theoretical model was also used to predict the properties of multichromophore structures made up of more polar and polarizable push–pull chromophores, and showed that stronger interchromophore interactions can heavily affect the individual optical responses. This suggests new routes for engineering highly NLO responsive multichromophore systems.

Introduction

Molecular materials are among the most promising candidates for advanced applications in electronics^[1] and photonics,^[2,3] and organic probes exhibiting high nonlinear optical (NLO) responses attract much attention in the field of biological imaging.^[4] The search for good candidates for these

applications relies both on enhancing the response at the molecular level and on the design and elaboration of supramolecular structures having optimized responses, by taking advantage of symmetry and environmental effects. As the synthetic approach evolves from the molecular to the supramolecular level, theoretical and interpretative models are needed to guide design at all stages. This is a critical issue, not only because real-world applications often involve condensed-phase systems ranging from solid-state devices to soft condensed matter (including biological systems), in which the individual molecular entities will interact, but also in a more fundamental vein. In fact, while structure–property relationships are quite actively and successfully investigated at the molecular level,^[5] supramolecular structure–property relationships remain an interesting open question, which deserves further analysis.^[1,6,7]

[a] Dr. F. Terenziani, Dr. O. Mongin, Dr. C. Katan, Dr. B. K. G. Bhatthula, Dr. M. Blanchard-Desce
Synthèse et ElectroSynthèse Organiques (CNRS, UMR 6510)
Institut de Chimie, Université de Rennes 1
Campus Scientifique de Beaulieu
Bât 10 A, 35042 Rennes Cedex (France)
E-mail: mireille.blanchard-desce@univ-rennes1.fr

 Supporting information for this article is available on the WWW under <http://www.chemeurj.org/> or from the author.

A great variety of structures can be generally classified as “supramolecules”, in spite of their possible different natures, ranging from crystals to films to multimolecular size-controlled assemblies to aggregates and multibranching or dendritic structures. However, all these architectures share the basic feature of being characterized by interactions between the “molecular bricks”. These interactions can be electrostatic in nature, originate from orbital overlap, or even involve active connectors between the components. While much experimental work has been devoted to the study of supramolecules,^[6] interpretative models are still scanty and relevant only to a few specific types of interacting systems.

A seminal theoretical work on the role of intermolecular interactions on the second-order optical properties of chromophoric molecular assemblies, which already dates back to more than ten years ago,^[8] demonstrated that the hyperpolarizability of *p*-nitroaniline dimers and trimers strongly depends on the relative molecular orientation of the chromophores and on intermolecular chromophore–chromophore interactions. This important result, confirmed by others,^[9,10] suggested some guidelines for the optimized design of chromophoric assemblies with large hyperpolarizabilities.^[11]

However, up to now, the still-unsolved problem is the ability to predict the properties of a supramolecular architecture starting from the properties of its building blocks. The benefit of such a bottom-up approach would be considerable, offering the possibility of taking advantage of the available knowledge on molecular properties and opening the way to the design of knowledge-based materials. *Ab initio* methods^[12] and semiempirical calculations^[13,14] are valuable tools for this aim, but at the expense of increased computational effort with increasing size of the system, especially when excited states, solvents or vibrational effects become important. In this respect, the study and modelling of size-limited and geometry-controlled molecular assemblies is not only important for the intrinsic properties of these structures, but also is a playground for modelling supramolecular interactions and testing proposed models. In fact, these assemblies have the basic ingredients of larger and more complex structures, with the advantage of being particularly suitable from the modeling point of view.

Simple models, based on a few states^[15–17] and on the choice of well-focussed interactions^[18] are also of great importance. These are, for example, the basic ingredients of the most widely used approach for interacting molecules: the excitonic model.^[19] This picture is apparently oversimplified, but it works well in describing the properties of aggregates of molecules interacting through their transition dipole moments,^[20] and it has also been successfully applied to model multipolar structures for NLO, in the case of weak interactions.^[21] However, the same model is inadequate for strongly interacting dipolar entities,^[22–24] as are often present in architectures optimized for second- or third-order NLO. In some cases the presence of nonelectrostatic intermolecular interactions (e.g., exchange interactions) is also a source of deviations from the predictions of the excitonic model.^[25–27]

Many supramolecular structures show enhanced NLO responses, but interpretative models have not often been applied or sufficiently tested. However, several (experimental) studies on different multichromophore systems showed that interchromophore interactions can play a significant role. In particular, increased SHG figures of merit for multichromophore structures have been reported in the literature.^[28–31] For example, donor– π –acceptor-functionalized calix[4]arenes showed up to 2.5-fold amplified figures of merit (per subchromophore) compared to the corresponding reference compounds.^[32] A striking example of increasing the figure of merit is a chromophore-functionalized polymer that shows 35-fold response per subchromophore with respect to the free chromophore.^[33] In these cases, the increased response was mainly due to a high degree of alignment of the functionalising chromophores: the hyperpolarizability of the supramolecular structures could be interpreted well by the oriented-gas model, even though, in the case of the polymer, a major contribution to the global dipole moment is made by the main polymer chain.^[33] In other examples, the response of multichromophore assemblies shows small^[34] or more sizeable deviations^[35,36] from additive behavior. These effects were ascribed to dipole–dipole coupling between subchromophores in functionalized cyclodextrins^[34] and dendrimers,^[36–38] and also to possible π – π interactions in functionalized calix[4]arenes.^[35,39] Another striking example of the role of interchromophore interactions is observed for cyclophane derivatives in which two dipolar push–pull stilbenes that are maintained in a forced relative orientation interact via through-space interactions.^[40,41] All these studies point to the importance of structural parameters (geometry, distance, nature of the chromophores) in multichromophore structures and call for further analysis.

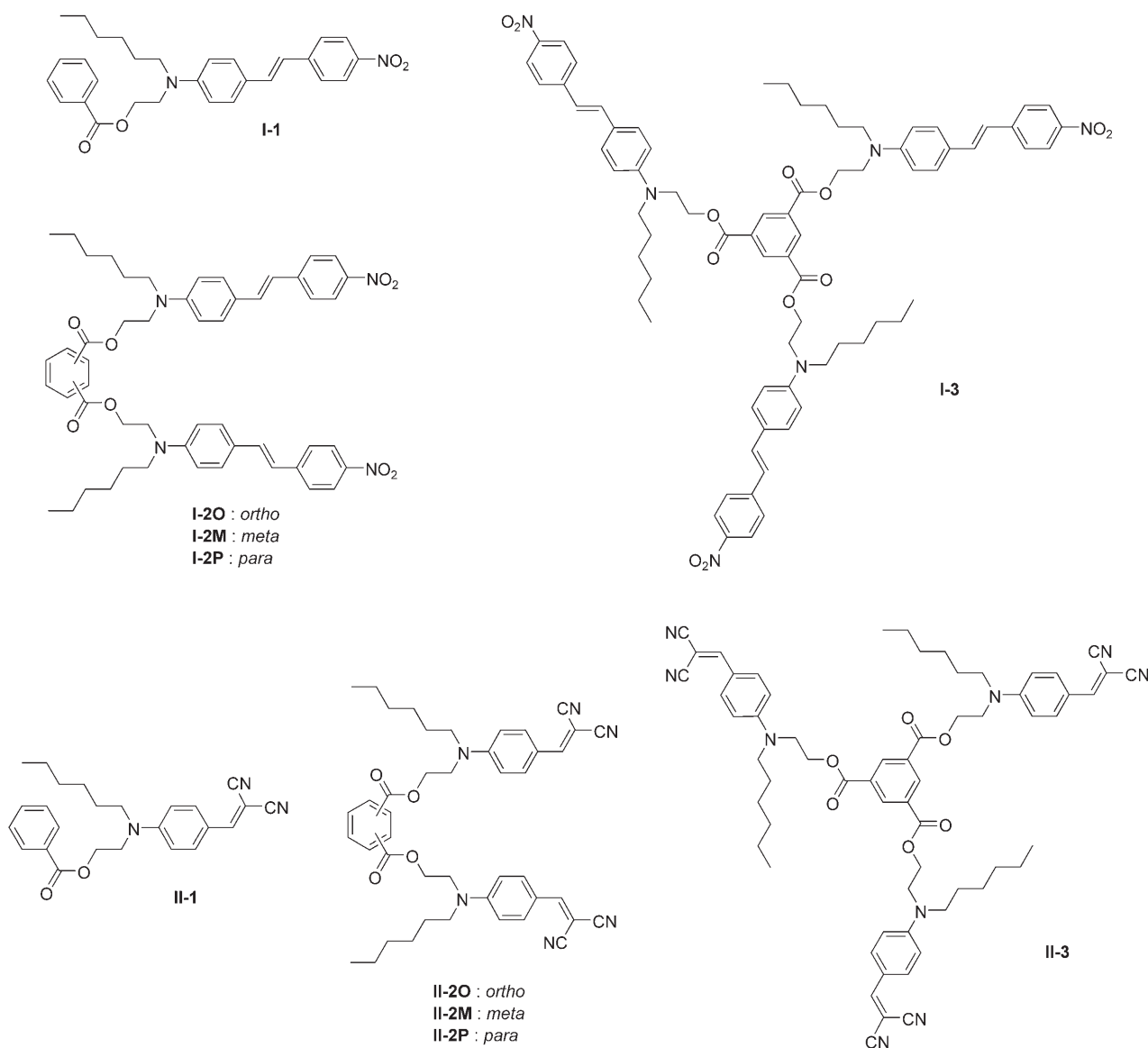
To address the problem of interaction effects on the properties of molecular multidipolar assemblies, we studied two series of homologous compounds, obtained by grafting one, two or three active dipolar chromophores onto a central phenyl core. In these model systems in which push–pull chromophores are assembled via covalent flexible linkers in close proximity, dipolar interactions between individual subchromophores are expected to influence both the conformation and the optical properties of the multichromophore nanoassemblies. From this perspective, chromophores with large dipole moments were selected. Such flexible multimer series provide valuable models for the investigation of confinement effects on the linear and nonlinear optical (NLO) responses of push–pull chromophores. Here we report their synthesis, spectroscopic characterization (absorption, fluorescence, solvatochromism) and experimental determination of their second-order NLO properties. Complementary to previously reported experimental and theoretical studies, our goal was to investigate how 1) the number of subchromophores, 2) the nature of the dipolar subchromophores (i.e., polarization and polarizability) and 3) geometrical constraints (such as fixed distance between specific parts of subchromophores) can influence the “supramolecular” effect.

The linear and nonlinear optical properties of the two series were interpreted by a recently proposed model which describes the responses of interacting polar molecules starting from the properties of the single chromophore.^[18,42] We demonstrate that interactions between subchromophores are responsible for their arrangement within the “supramolecules” and thus fix the responses of the assemblies. For the studied series, this is true even though interchromophore distances are too large to sizeably affect the individual responses of each constituent subchromophore. We also show, through simulations that, at shorter distances or for more polar and/or polarizable subchromophores, the geometry and optical response of the multichromophore assemblies are highly and nontrivially affected by subchromophore interactions. This opens the route towards cooperative multichromophore assemblies in which the NLO responses of the individual subchromophore components would also be enhanced and much more efficient molecular assemblies would result.

Results

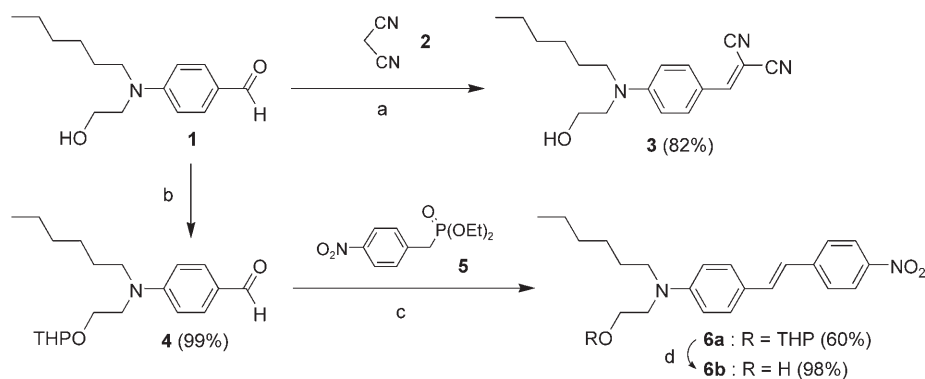
Model systems: Two series of size-controlled multichromophore assemblies were synthesized by functionalising a central phenyl core with two or three push-pull chromophores with the same electron-releasing amino group and by two different electron-withdrawing moieties: a nitrophenyl group (Series I) or a dicyanovinyl moiety (Series II). The chromophores were grafted to the central core through flexible connectors that act as “passive” spacers between the active chromophores. This allows electrostatic forces to be singled out as the source of intermolecular interactions. In addition, the chosen spacers maintain spatial proximity between subchromophores and thus allow through-space dipole–dipole interaction to take place while providing the required flexibility for orientational freedom.

Three types of dimers were prepared by grafting the two subchromophores onto the central core in *ortho*, *meta* or *para* positions. This allows the distance between subchromo-



phores to be modulated and the effect of interchromophore distance on the properties of the multichromophoric assemblies to be studied. The spectroscopic and second-order NLO properties of the dimers and trimers in each series were studied and compared with the properties of the corresponding monomeric model compounds obtained by attaching a single subchromophore to the same central core through the same connector. The effects of intermolecular interactions on the geometry and properties of the assemblies were deduced and rationalized.

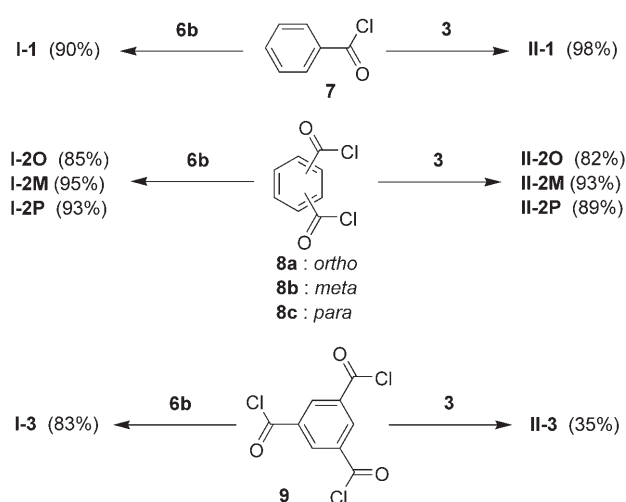
Synthesis: Graftable chromophoric building blocks **3** and **6b** were synthesized from the same precursor, that is, aldehyde **1** (Scheme 1). The NLO-phore **3** was prepared by Knoevenagel condensation of **1** with malononitrile (**2**), whereas **6b** was obtained in a three-step sequence involving protection of the alcohol functionality of **1** as an acetal, Horner–Wadsworth–Emmons condensation with phosphonate **5** and de-



Scheme 1. Synthesis of graftable chromophoric bricks **3** and **6b**. a) **2**, EtOH, reflux, 18 h; b) dihydropyran, PPTS, CH₂Cl₂, 20 °C, 15 h; c) **5**, NaH, THF, 20 °C, 16 h; d) HCl, CH₂Cl₂/EtOH, reflux, 17 h.

protection of the acetal (Scheme 1). By esterifying both alcohols (**6b** and **3**) with acyl chlorides **8a–c** and **9**, two series of di- and trichromophore assemblies (**I** and **II**, respectively) were obtained. Monochromophore models **I-1** and **II-1** were obtained by reaction of **6b** and **3** with benzoyl chloride (Scheme 2).

Linear optical properties: The UV/Vis absorption and fluorescence spectra of **I-1**, **I-2O**, **I-2P** and **I-3** were recorded in toluene, chloroform and acetone. Spectra of **II-1**, **II-2M**, **II-2P** and **II-3** were recorded in toluene, CHCl₃ and dimethyl sulfoxide (DMSO). A fourth solvent (triacetin) was used for **I-1**. The solvatochromic absorption and emission properties of **I-1** and **II-1** are reported in Figure 1 and Table 1, while the solvatochromism of dimers and trimers is available as Supporting Information. The solvatochromic behavior of each compound in a series is nearly the same, characterized by a red shift of both absorption and fluorescence bands with increasing solvent polarity, an effect which is more pronounced for fluorescence spectra.



Scheme 2. Synthesis of the two series of multichromophoric assemblies. Reaction conditions: NEt₃, CH₂Cl₂, 20 °C, 4 h, then reflux, 1 h.

Figure 2 compares the spectra of the compounds of series **I** (a) and **II** (b) in CHCl₃. Spectra in the other solvents are available as Supporting Information. Slight effects on absorption and fluorescence bands are recognizable, due to subchromophoric interactions. In particular, a small blue shift is observed going from the monomer to the multimers in the case of both series, whereas a decrease of oscillator strength (per subchromophore) is observed in the case of series **II** (see also Table 2). The decrease in maximum extinction coefficient is accompanied by a slight broadening of the spectrum. This (inhomogeneous) broadening on going from the monomer to the trimer is most probably linked to the larger conformational disorder in the multimers.

Fluorescence quantum yields were measured by using fluorescein in 0.1N NaOH as reference ($\phi_{\text{ref}}=0.90$).^[43] Compounds of series **I** have significant quantum yields in toluene, which vary from about 80% for the monomer down to about 20% for the trimer. In CHCl₃ and acetone the quantum yields are very low (about 3 and 1%, respectively) for all members of the series. Series **II** has very weak quantum yields, always lower than 1%.

Dipole moments: Dipole moments μ of all the products of series **I** and of **II-1** were determined from dielectric and refractive index measurements in CHCl₃, by means of the Debye formula.^[44] The measured values are reported in Table 4. Compound **II-1** has a larger dipole moment than **I-1**, even though the length of the dipole can be estimated to

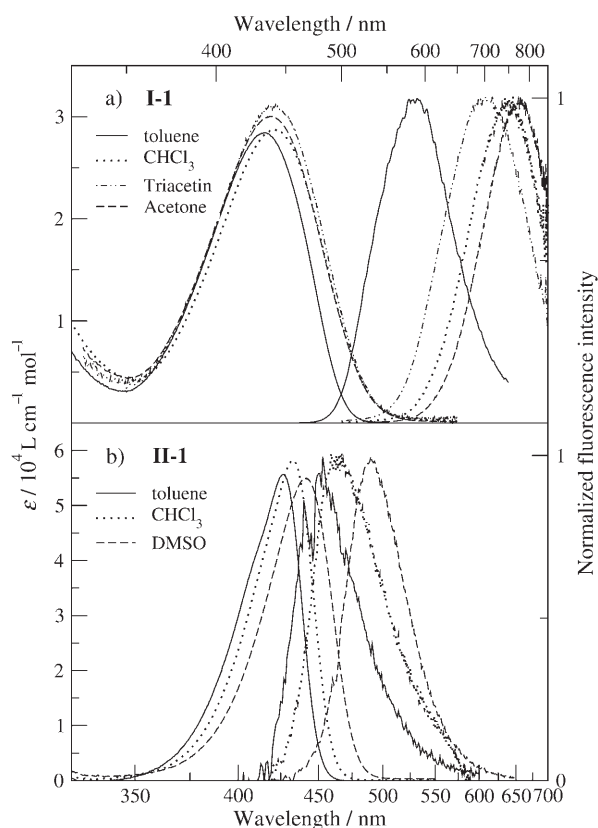


Figure 1. Absorption and fluorescence solvatochromism of the monomeric models: a) **I-1**; b) **II-1**.

Table 1. Absorption and fluorescence properties of **I-1** and **II-1** in different solvents: maximum absorption wavelength λ_{abs} , oscillator strength f , emission wavelength λ_{em} at the maximum, and fluorescence quantum yield ϕ .

	Solvent	λ_{abs} [nm]	f	λ_{em} [nm]	ϕ
I-1	toluene	433	1.6	585	0.84
	CHCl_3	440	1.6	750	0.031
	acetone	439	1.7	775	0.015
II-1	toluene	425	1.6	450	0.001
	CHCl_3	433	2.0	465	0.002
	DMSO	440	2.1	490	0.004

be shorter. This suggests a more pronounced charge-transfer character of **II-1** in the ground state, probably due to the stronger electron-withdrawing character of the dicyanovinyl group with respect to the nitro group.

Values for series **I** allow the conclusion that all the multimers have a large dipole moment (from 12 to 15 D), which indicates a nonrandom spatial organization of the subchromophores grafted to the central core. In particular, by assuming a V-shaped configuration for the dimers, and a calyx-like shape for the trimers (see Figure 3), the angle formed by each subchromophore with the main symmetry axis of the assembly can be estimated. Under the assumption that the dipole moment of each subchromophore in the

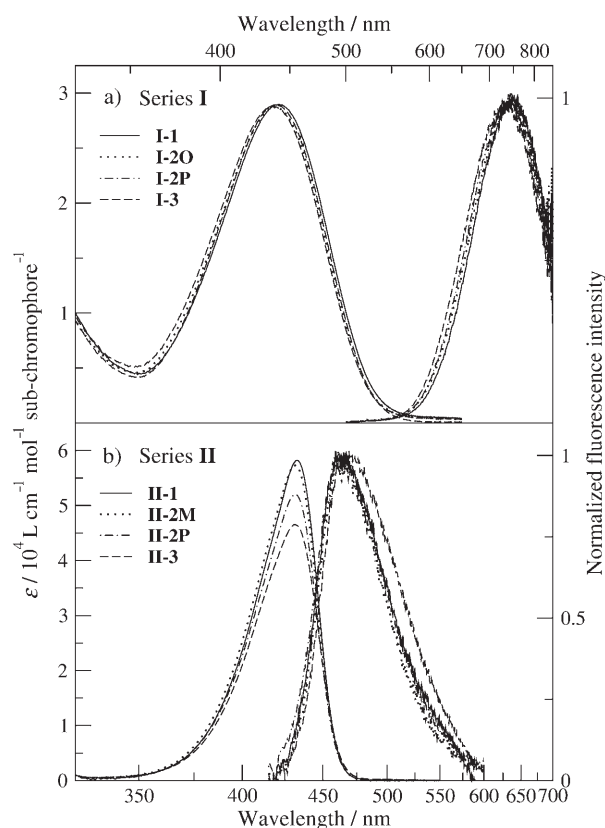


Figure 2. Absorption (per subchromophore) and fluorescence spectra in chloroform: a) series **I**; b) series **II**.

Table 2. Absorption and fluorescence properties of analogous compounds from series **I** and **II** in CHCl_3 : maximum absorption wavelength λ_{abs} , oscillator strength f , emission wavelength λ_{em} at the maximum, and fluorescence quantum yield ϕ .

	λ_{abs} [nm]	f	λ_{em} [nm]	ϕ
I-1	440	1.6	750	0.031
I-2O	438	3.2	745	0.036
I-2P	436	3.3	740	0.025
I-3	438	4.8	735	0.032
II-1	433	2.0	465	0.002
II-2M	430	4.0	465	0.002
II-2P	430	3.8	465	0.002
II-3	430	5.1	470	0.004

Table 3. Parameters [eV] of the two-state model (see text) that allow reproduction of the experimental absorption and fluorescence spectra of **I-1** and **II-1**. The three values for ϵ_{or} correspond to toluene, CHCl_3 , and acetone, respectively, for **I-1**; and to toluene, CHCl_3 , and DMSO, respectively, for **II-1**.

	z_0	$\sqrt{2}t$	ω_v	ϵ_v	Γ	ϵ_{or}	ϵ_c
I-1	1.3	0.6	0.12	0.52	0.06	0/0.35/0.40	0.15
II-1	1.0	1.1	0.16	0.21	0.05	0.16/0.27/0.43	–

assembly is not strongly affected by intermolecular interactions, the following angles were calculated: 45° for **I-2O**, 35° for **I-2M**, 40° for **I-2P** and 55° for **I-3**.

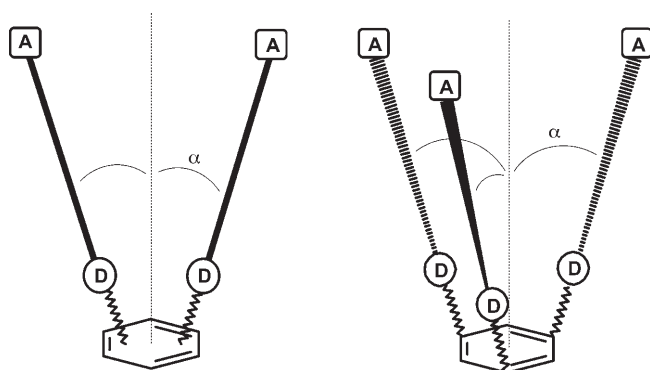


Figure 3. Schematic representation of the supramolecular structures. Zigzag lines correspond to the linkers between the central core and the active subchromophores. Subchromophores are represented by rods bearing electron-donor (D) and electron-acceptor (A) groups. For dimers and trimers C_{2v} and C_{3v} symmetries are assumed, respectively; α is the angle formed by each subchromophore with respect to the main symmetry axis (dashed line).

Second-order NLO properties: The second-order NLO responses of all products were measured in CHCl_3 by the electric-field-induced second-harmonic generation (EFISHG) technique, operating at $1.9 \mu\text{m}$.^[45] This method, which can only be used for solutes having a nonvanishing dipole moment, provides access to the product $\mu\beta(2\omega)$, where β is the vector component of the β tensor in the direction of the dipole moment (z), usually called β_z . In the following all the reported and discussed β values correspond to this quantity, except where explicitly specified. The $\beta(2\omega)$ values can be calculated provided the dipole moments are known. The corresponding static values $\beta(0)$ can also be estimated by using the two-state model^[46] [Eq. (1)]

$$\beta(0) = \frac{(\omega_{\text{abs}}^2 - \omega^2)(\omega_{\text{abs}}^2 - 4\omega^2)}{\omega_{\text{abs}}^4} \beta(2\omega) \quad (1)$$

The EFISHG figure of merit $\mu\beta(0)$ is then accessible. All results are reported in Table 4 according to the X convention as defined in reference [47]. The multichromophore strategy leads to amplification of the figure of merit by up to a factor of four for the trimer of series **II**, with a net gain with respect to the increased molecular weight. Indeed all multimers show higher normalized figure of merit $\mu\beta(0)/M$ than the corresponding monomer. Interestingly, the enhancement seems to increase with increasing number of subchromophores in the nanoassembly and with increasing polarity of the subchromophores.

Discussion

Solvatochromism: The solvatochromic behavior of all the

studied products is typical of transitions involving an excited charge-transfer state having a larger dipole moment than the ground state.^[48] A rough assessment of the value of $\Delta\mu$ (the difference between the dipole moment of the excited and ground states) can be derived from $\beta(0)$ by using the two-level model, starting from the measured values of the transition frequency and dipole moment.^[46] This estimate leads to $\Delta\mu$ values of 9.1 and 3.6 D for **I-1** and **II-1**, respectively. This also confirms the assumption of a more pronounced charge-transfer character for the ground state of **II-1** with respect to **I-1**.

The spectra of **II-1** can be reproduced by the two-state model with Holstein coupling to an effective molecular vibration and solvation interaction. The model is detailed in reference [49] and summarized in the Experimental Section. The fit allows estimation of the model parameters: the energy difference between the neutral and the zwitterionic basis states $2z_0$, the mixing matrix element $-\sqrt{2}t$, the vibrational frequency ω_v and the vibrational relaxation energy ϵ_v of the effective coupled mode. To reproduce the spectra, Gaussian band shapes were chosen with half-width at half-maximum Γ . Another parameter is needed to describe the solvent polarity: the solvent relaxation energy ϵ_{or} , which is the only parameter that is allowed to change from one solvent to another. Spectra of **II-1** can be reproduced by fixing the parameters listed in Table 3. To quantitatively reproduce the absorption intensity, the value $\mu_0 = 20.5$ D was fixed for the dipole moment of the zwitterionic basis state. The fit of the spectra is shown in Figure 4b. These parameters correspond to a degree of charge transfer ρ in the ground state ranging from 0.15 in toluene to 0.16 in DMSO.

The model, when allowed to fully account for molecular polarizability at all orders, also estimates different degrees of charge transfer for the molecule when slow coordinates (vibrational and solvation degrees of freedom) are in equilibrium with the electronic distribution relevant to the ground or excited state.^[49,50] This mechanism of interaction is typically nonlinear, since the configuration of slow degrees of freedom depends on the molecular electronic distribution, which in turn is affected by the configuration of slow degrees of freedom. This leads to the following degrees of charge transfer ρ in the Franck–Condon ground state, which is relevant to the fluorescence process: 0.20, 0.22 and 0.25 in toluene, CHCl_3 and DMSO, respectively. This means that in

Table 4. Dipole moments and hyperpolarizabilities of all compounds of series **I** and some compounds of series **II**. The last two columns report calculated values. Values in parentheses correspond to the ratio between the response of the relevant multimer and the response of the monomer.

Compound	μ [D]	$\mu\beta(2\omega)$ [10^{-48} esu]	$\mu\beta(0)/M$ [10^{-48} esu mol g^{-1}]	$\beta(2\omega)$ [10^{-30} esu]	$\mu\beta(2\omega)_{\text{calcd}}$ [10^{-48} esu]	$\beta(2\omega)_{\text{calcd}}$ [10^{-30} esu]
I-1	8.7	390	0.61	45	258	153
I-2O	12.3 (1.4)	720 (1.8)	0.62	58 (1.3)	488 (1.9)	209 (1.4)
I-2M	14.2 (1.6)	790 (2.0)	0.68	56 (1.2)	578 (2.2)	228 (1.5)
I-2P	13.2 (1.5)	900 (2.3)	0.77	68 (1.5)	632 (2.4)	239 (1.6)
I-3	15.1 (1.7)	1260 (3.2)	0.75	83 (1.8)	733 (2.8)	255 (1.7)
II-1	9.7	180	0.35	19	214	67
II-2M	–	350 (1.9)	0.36	–	544 (2.5)	107 (1.6)
II-3	–	715 (4.0)	0.52	–	831 (3.9)	130 (1.9)

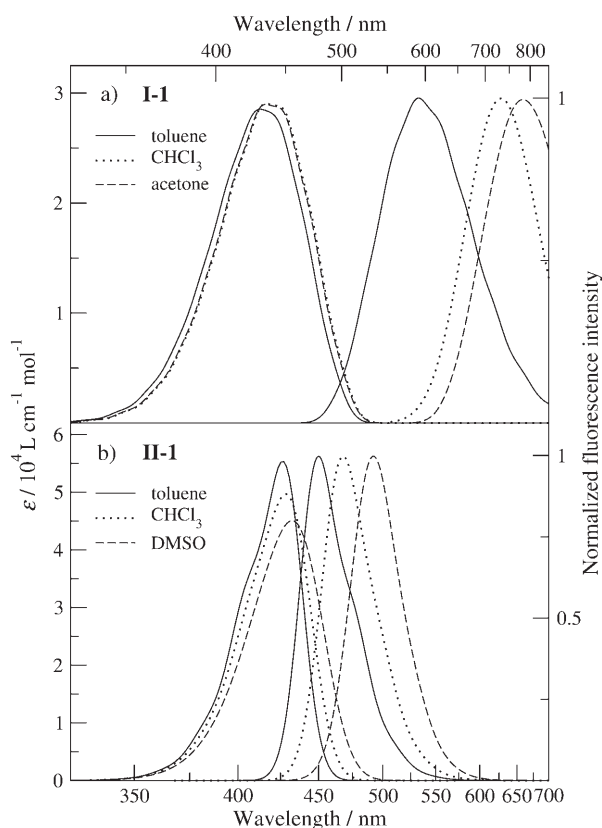


Figure 4. Calculated absorption and fluorescence solvatochromism of the monomeric models: a) **I-1**; b) **II-1**. Parameters in Table 3 were used.

the geometry relevant to the fluorescence process, the molecule has a more polar and polarizable ground state than in the geometry relevant to the absorption process.

The fit of the spectra of **I-1** is somewhat more difficult. Spectra in Figure 1a show that the Stokes shift is very large even in an almost nondipolar solvent like toluene. This suggests the presence of another coupled degree of freedom, different from a molecular vibration and from the solvation coordinate. Due to the nonrigid structure of the relevant chromophore, this coordinate is probably a conformational degree of freedom, so that fluorescence likely stems from a so-called twisted intramolecular charge transfer state. This hypothesis is indirectly confirmed by spectra recorded in triacetin, a very viscous solvent (dot-dashed lines in Figure 1a): in fact, even though triacetin is more polar than CHCl_3 , the Stokes shift in this solvent is smaller than in chloroform, and this suggests that the high viscosity hinders to some extent conformational reorganization in the excited state. Conformational coordinates are different in nature from molecular vibrations or from solvation degrees of freedom: while the last-named coordinates affect diagonal terms in the Hamiltonian, a conformational coordinate modulates the mixing matrix element (the charge transfer integral) between the basis states.^[51] This type of coupling was already modelled to successfully describe the spectra of phenol blue, another flexible chromophore.^[49] Here we use this extension of the model, by introducing the relevant additional param-

eter: the conformational relaxation energy ϵ_c . The first effect of this coupling is an increased Stokes shift, because the equilibrium conformational coordinate is different for the ground and excited states. In addition, a Boltzmann distribution of conformations must be accounted for at finite temperature, since the conformational coordinate is characterized by very low frequency (typically in the far-infrared/microwave region) that leads to an additional inhomogeneous broadening of the absorption and emission bands.

By fixing the parameters in Table 3, the spectra of **I-1** in all solvents can be reproduced.^[52] The value of μ_0 was fixed to 33 D. The corresponding degrees of charge transfer are lower than for **II-1**, on the order of 0.05 in all the solvents. This is again a confirmation of the weaker electron-withdrawing power of the nitro group compared to the dicyanovinyl group. The solvatochromic effect is also smaller in absorption and larger in fluorescence in series **I** than in series **II**, and this points to the more neutral nature of the chromophore in series **I**.

Interchromophore effect: Interchromophore interactions for the two studied series are purely electrostatic in nature. The spacers connecting each subchromophore to the central phenyl core are “passive”, that is, they prevent extension of conjugation from one subchromophore to another. Moreover, the estimated distance between the grafted subchromophores is large enough to hinder overlap between molecular orbitals of different subchromophores. In addition, in both cases interactions are weak, as demonstrated by the small variations of absorption and fluorescence spectra on going from the monomers to the dimers to the trimer. This is due to their strongly dominant neutral nature and also to the molecular architecture. In the chosen multichromophore structures, chromophores are linked to the central core through one end, while the other end is completely free, so that the subchromophores have the possibility to adopt the relative orientation that minimises repulsive interactions. This leads to noncentrosymmetrically self-organized structures, as proven by the large dipole moments measured even in the case of trimers and *para* dimers. This intrinsic asymmetry results in significant second-order nonlinearity, that is, even in the case of weak interaction, when the individual optical responses of the subchromophores within the nanoassembly are not much affected, the dipolar interchromophore interactions play an important role by controlling their relative orientation and thus the overall architecture of the nanoassembly.

By using a simple electrostatic model, it is possible to plot the dependence of the interaction energy on the angle formed by the subchromophores. The dipole approximation could be used, but it would not permit cases in which the chromophores have different lengths (e.g., series **I** and series **II**) to be distinguished. Hence, here we prefer to assign positive/negative charges to the donor/acceptor ends and model the interactions by estimating the interchromophore distance (at the donor ends) and the length of each chromophore (between donor and acceptor groups). We as-

sumed a V-shaped configuration for dimers (C_{2v} charge symmetry) and a calyx-like shape for trimers (C_{3v} charge symmetry), as sketched in Figure 3. We fixed the distance between the donor ends at 13, 15, and 17 Å respectively for *ortho*, *meta* and *para* positions, and imposed a length of 10 and 8 Å, respectively, for the chromophores in series **I** and **II**. By minimising the electrostatic energy of interaction, we predict the following angles formed by each subchromophore with respect to the principal symmetry axis of the assembly: 46° for **I-2O**, 41° for **I-2M**, 38° for **I-2P**, 55° for **I-3**; 40° for **II-2O**, 36° for **II-2M**, 33° for **II-2P**, and 47° for **II-3**. The deviation between the two series results from the difference in chromophore length. The estimated angles compare well with the angles derived from the experimental dipole moments of (multi)chromophores of series **I**.^[53] This simple procedure is already a clear demonstration that interchromophore electrostatic interactions determine the relative orientation of subchromophores and hence the supramolecular conformation of the assembly.

Note that the strength of the electrostatic interaction that can be estimated between subchromophores in the assemblies is at least one order of magnitude higher than the interaction between each subchromophore and the static electric field applied for the EFISHG experiment (typically on the order of 10^6 V m⁻¹). For this reason the geometry of the multichromophores can be considered as independent of the applied electric field, and the nanoassemblies can be regarded as independent units that interact with the field itself via their global dipole moment.

To further validate the proposed approach, in the following we show spectra calculated for dimers and trimers, as well as the calculated β values for all members of the two series. The extension of the two-state Mulliken model to describe interacting chromophores has been recently proposed.^[18,54] This approach is different from the standard excitonic model, since it allows the properties of the “supramolecule” to be calculated by starting from the parameters estimated for the isolated (or solvated) chromophore unit and from the geometry of the assembly. This is due to the fact that the molecular (hyper)polarizability is fully accounted for, so that environmental effects are self-consistently taken into account. Another noteworthy difference to the standard excitonic approach is the fact that all electrostatic interactions are considered, not only those arising from the coupling of the transition dipole moments; the latter approximation is strictly valid only for nondipolar molecules. This model for interacting polar and polarizable chromophores has been further extended to account for molecular vibrations and solvation,^[42,55] to allow comparison with experimental measurements. Along these lines, the calculations reported hereafter were performed.

Figure 5 shows spectra calculated for series **II**. For the multimers, the same parameters as deduced for the monomer were used, with additional geometrical parameters, that is, interchromophore distances and angles, as obtained by minimising the interactions. In this case interactions are weak (interchromophore distances are about twice the chro-

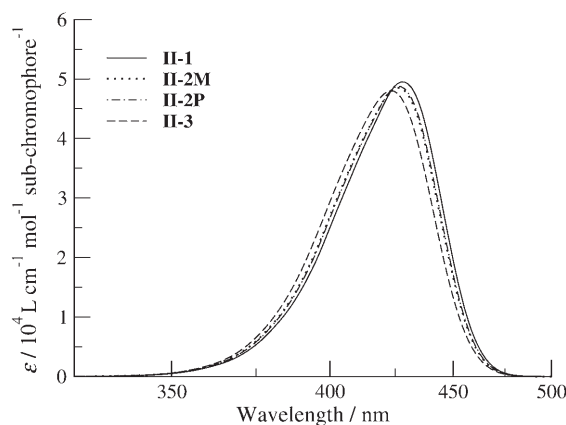


Figure 5. Calculated absorption spectra (per subchromophore) of series **II** (chloroform). Parameters in Table 3 were used. For **II-3** inhomogeneous broadening has not been taken into account, and a half-width at half-maximum of 0.11 eV has been imposed.

mophore length), so that multichromophore effects are also weak: subchromophore polarity only varies by 1 and 2%, respectively, for the trimers of series **I** and **II** with respect to the monomeric analogue. The main characteristics of the spectra are reproduced, such as the small blue shift of the band and the small decrease in oscillator strength from the monomers to the multimers. Experimental spectra of dimers and trimer are somewhat additionally broadened, but this can be associated with the higher geometrical disorder for the multimers. These calculated spectra are confirmation that the fixed geometrical parameters are reliable.

A further test of the chosen parameters and of the proposed interpretation is given by comparison of experimental and calculated β values. Calculated $\mu\beta(2\omega)$ and $\beta(2\omega)$ are reported in Table 4. The agreement is not quantitative with respect to the individual values, but the trend within each series is well reproduced, as shown by the ratios between the response of the multimers and the response of the corresponding monomer (values in parentheses in Table 4). The nonquantitative agreement of the individual values is mainly due to the evaluation of the dipole moment in the ground and excited states. Both the transition energy and the transition dipole moment are well reproduced (as demonstrated by the good agreement between experimental and calculated spectra). On the contrary, the ground-state dipole moments fixed by the chosen molecular parameters strongly underestimate the measured values: 1.6 D and 3.2 D calculated for **I-1** and **II-1**, versus experimental values of 8.7 and 9.7 D, respectively. This quite large discrepancy is somewhat surprising, since the calculated (permanent) dipole moments allow the solvatochromic behavior of all compounds to be correctly reproduced. A possible reason may be related to the fact that the dipole moments estimated from the fit of the spectra are related to the polarizable (and hence responsive) part of the skeleton only, while the measured values correspond to the total dipole moments. Furthermore, the contribution of the connecting spacers to the total dipole moment may be nonnegligible, and their contribution is

more important for smaller dipole moments of the grafted chromophore (more important for series **I** than for series **II**). The same problem also afflicts the excited state, for which calculations overestimate the dipole moment. Despite these discrepancies, we observe good agreement between the experimental and calculated values of the ratio between the nonlinear responses of the multimers and of the corresponding monomer (Table 4).

The sizeable increase in the β value from *ortho* dimer to *meta* dimer to *para* dimer (series **I**) indicates that the distance between subchromophores influences the self-arrangement of the dipolar subchromophores within the nanoassembly and thus its second-order optical response. The non-random spatial self-organization results in an increase in β response from the monomer to the multimers by a factor on the order of 1.5–2. This, in combination with the increased dipole moment in the dimers and trimers, leads to an amplification of the figure of merit $\mu\beta$ by up to a factor of four. The amplification is more important for series **II** than for series **I**, because of the smaller angles imposed by interchromophore interactions, which result from the difference in length of the corresponding monomers. Interestingly, for both series the trimer shows improved performance as compared to the dimeric analogues. Hence, for the same interchromophore distance (i.e., when comparing trimers with *meta* dimers), the multichromophore strategy provides improved second-order NLO response with increasing number of subchromophores in the nanoassembly.

Conclusions and Perspectives

We have addressed the properties of multidipolar structures by experimental measurements of linear and nonlinear optical properties, and with a recently proposed theoretical model for interacting polar and polarizable molecules. Multichromophore assemblies were obtained by grafting one, two or three active chromophores onto a central passive core. In the studied cases, responses of multimers are almost additive, in the sense that an oriented-gas model can account for the properties of the assemblies. More importantly, we demonstrated that the relative orientation of subchromophores is dictated by intermolecular interactions, so that interactions are the driving force in determining the properties of the assembly, even when they are fairly weak. Interbranch interactions are thus responsible for nonrandom self-arrangement of the subchromophores grafted to the central core, which lead to an increased dipole moment of the supramolecular assemblies with respect to the monomeric analogues. The increase in dipole moment has a twofold advantage. It is responsible for better molecular orientation and thus a higher value of the global order parameter, which possibly results in higher bulk susceptibilities. Moreover, at the microscopic level this effect can lead to increased figures of merit $\mu\beta$ per subchromophore: in our case an increase of up to 30% (for compound **II-3**) was observed.

Some reports in the literature suggest that strong interactions between chromophores can lead to large deviations from simple additive contributions of active chromophores. The analysis here is a case study, relevant to the limit of weak interactions; but the adopted model can be exploited to predict the properties of strongly interacting chromophores, since it fully takes into account the molecular polarizability. In fact, dipolar chromophores are highly responsive to any change in the environment (as demonstrated by their pronounced and nontrivial solvatochromism), so that the properties of multichromophore systems are expected to strongly depend on relative intermolecular orientation and distance.^[8,13,18] The stronger the interactions and the more polarizable the chromophores, the larger these “environmental” effects will be.^[18] Figure 6 shows examples of what

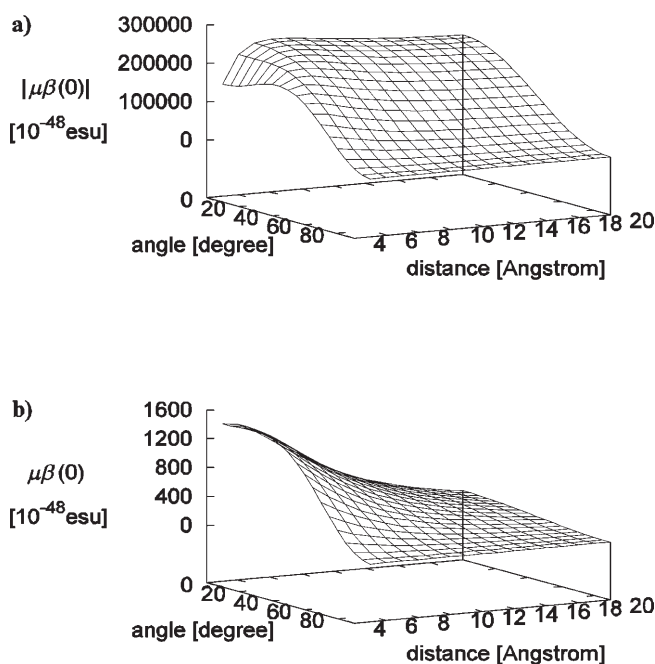


Figure 6. Angle and distance dependence of the SHG figure of merit, calculated for a dimer (C_{2v} symmetry) of a) $C_{16}H_{33}Q-3CNQ$ molecules in $CHCl_3$ (parameters estimated in reference [56]) and b) molecules that are in the cyanine limit when isolated.

is expected for more polar and polarizable interacting chromophores. Figure 6a shows the figure of merit (absolute value) calculated for a dimer (C_{2v} symmetry) of molecules that are almost zwitterionic when isolated in solution. Parameters are relevant to the chromophore $C_{16}H_{33}Q-3CNQ$, as reported in reference [56]. In this case, at an intermolecular distance of about 10 Å and a corresponding equilibrium intermolecular angle (ca. 42°), the response of the dimer is almost three times the response of the isolated molecule, because polarization effects sum up to oriented-gas effects in determining the properties. For this same dimer, a figure of merit five times larger than that of the monomer is expected for parallel molecules at an intermolecular distance of 8 Å

(without polarizability effects, the gain factor could not be larger than four). Figure 6b is relevant to push–pull chromophores at the cyanine limit when isolated. This means that their first hyperpolarizability is vanishing. However, due to intermolecular interactions, large SHG figures of merit can be obtained. This is a striking example of the importance of polarizability effects on the properties of interacting systems: even starting from nonresponsive molecules, highly responsive assemblies could be achieved. Hence, the same model molecule, arranged in assemblies of different fashions (relative distance, orientation, etc.) can behave in quantitatively and qualitatively different ways. The ability to correctly take into account all these ingredients in the design and synthesis of supramolecular structures in a knowledge-based (or bottom-up) approach will allow geometrical degrees of freedom to be tailored to maximise the desired responses. In this respect, we are currently working on the engineering of multichromophore systems made up of strongly polar and/or polarizable chromophores, to exploit their self- or pre-arrangement, as well as a possible self-improving mechanism of the desired property.

Experimental Section

Spectroscopic measurements: UV/Vis spectra were recorded on a Jasco V-570 spectrophotometer on about 10^{-5} M solutions. Fluorescence measurements were performed on dilute solutions (ca. 10^{-6} M) with an Edinburgh Instruments (FLS 920) spectrometer in photon-counting mode. For series II, Raman emission lines of the solvent were subtracted from the emission signal. Fluorescence quantum yields were measured by using fluorescein in 0.1 N NaOH as standard (quantum yield $\phi = 0.90$).^[43] Solvents were of spectroscopic grade. All measurements were carried out at room temperature.

Dipole moment measurements: Permanent dipole moments were determined by means of a WTW dipole meter (type DM01) with a capacitance cell for liquids and a capacitance-measuring electronic bridge.

NLO measurements: Measurements of β were performed by the EFISHG technique.^[45] The EFISHG experiment allows determination of the mean microscopic hyperpolarizability γ_0 [Eq. (2)].

$$\gamma_0 = \gamma(-2\omega; \omega, \omega, 0) + \mu\beta(-2\omega; \omega, \omega)/(5kT) \quad (2)$$

The first term is the scalar part of the cubic hyperpolarizability tensor, whereas the second originates from the partial orientation of the permanent dipole moment μ in the static field. The orientational contribution is usually assumed to be the predominant component in the case of polar charge-transfer molecules. The product $\mu\beta(2\omega)$ is thus directly inferred. EFISHG measurements were conducted with a Q-switched Nd³⁺:YAG laser emitting pulse trains and operating with the first Stokes radiation, at 1.907 μm , of the YAG 1.064 μm emission generated in a hydrogen Raman cell. These experiments were performed by using, for each molecule, solutions of increasing concentration in chloroform. Measurements were calibrated relative to the pure solvent. The experimental accuracy does not exceed 5%. The reported β values follow the *X* convention as defined in reference [47].

Theoretical model and calculations: Push–pull chromophores are molecules made up of an electron-donor and an electron-acceptor group connected by a π -conjugated bridge. They are characterized by a low-energy transition (in the visible region) with high intensity, linked to charge transfer from the donor to the acceptor moiety. For this reason they are usually and successfully described as resonating between two basis states: the neutral and the zwitterionic structure, so that a two-level model is

sufficient for describing the basic physics of these molecules. The theoretical approach adopted here is based on the two-state Mulliken model,^[57] extended to account for Holstein coupling to molecular vibrations and solvation interaction. For a single chromophore in solution the relevant Hamiltonian reads as Equation (3),^[50]

$$h = 2z_0\hat{\rho} - \sqrt{2}t\hat{\sigma}_x + \sum_i \left[\frac{1}{2}(\omega_i^2 Q_i^2 + P_i^2) - \sqrt{2}\varepsilon_i \omega_i Q_i \hat{\rho} \right] \quad (3)$$

where z_0 and t are the parameters of the two-state model: $2z_0$ is the energy difference between the neutral and zwitterionic basis states, and $-\sqrt{2}t$ the mixing matrix element (charge-transfer integral); $\hat{\rho}$ is the operator that counts electrons on the acceptor site; and $\hat{\sigma}_x$ is one of the Pauli spin operators. The expectation value $\rho = \langle \hat{\rho} \rangle$ measures the weight of the zwitterionic structure in the ground state, and hence represents the molecular polarity. In fact, following Mulliken, a dipole moment μ_0 can be associated to the zwitterionic basis state, neglecting all other contributions. In this way, the ground-state dipole moment is given by $\mu_0\rho$, and the excited state dipole moment by $\mu_0(1-\rho)$. Transition energy and dipole moments are respectively given by $\hbar\omega_{\text{CT}} = \sqrt{2}t\sqrt{\rho(1-\rho)}$ and $\mu_{\text{CT}} = \mu_0\sqrt{\rho(1-\rho)}$.

In the above Hamiltonian the summation runs over coupled modes (of coordinate Q_i , momentum P_i and frequency ω_i), that is, coordinates along which the potential energy surfaces relevant to the two basis states are displaced. The parameter ε_i measures the relaxation energy of the relevant mode. Coupled modes can be molecular vibrations, or also a solvation coordinate (in the case of polar solvents). Here we reproduce experimental spectra by use of a single coupled molecular vibration (of frequency ω_v and relaxation energy ε_v) and a solvation coordinate (of relaxation energy is ε_{or}). The frequency of the solvation degree of freedom (which is very low, typically in the far-infrared/microwave region) need not be fixed, since this mode can be treated as a classical coordinate.^[58] At finite temperature a Boltzmann distribution along this coordinate must be accounted for, which is the origin of inhomogeneous broadening of spectra in polar solvents.^[49,58] Along the vibrational coordinate, the potential energy surfaces relevant to the two basis states are chosen as harmonic and with the same frequency. However, as a result of diagonalization, potential energy surfaces are no longer harmonic for the ground and excited states, and they are softened and hardened, respectively.^[58] In the adiabatic approximation, the electronic problem corresponds again to a two-state problem, but with the parameter z_0 self-consistently renormalized: $z_0 \rightarrow z_0 - (\varepsilon_v + \varepsilon_{\text{or}})\rho$ if slow degrees of freedom are in equilibrium for the ground state, and $z_0 \rightarrow z_0 - (\varepsilon_v + \varepsilon_{\text{or}})(1-\rho^*)$ if slow degrees of freedom are in equilibrium for the excited state.^[50,58] The self-consistency corresponds to the system (hyper)polarizability. One of the consequences of the electronic polarizability is just the different degree of charge transfer ρ in the case of different geometries of slow variables: a ground-state polarity ρ relevant to the absorption process and a ground state polarity ρ^* relevant to the fluorescence process. This allows nonspecular absorption and fluorescence spectra to be accounted for.^[49,50]

The vibrational problem is solved exactly (for the ground and excited electronic states) on the basis of a harmonic oscillator of frequency ω_v centered at the relevant equilibrium position.^[59] The vibrational matrix is diagonalized on a truncated basis sufficient to achieve convergence.^[60] As for semiempirical models, all parameters are fixed so as to best reproduce experimental spectral features. Spectra were calculated by associating to each vibronic transition a Gaussian lineshape.

For flexible chromophores another degree of freedom describing conformational motion must be accounted for. Such a mode tunes the charge-transfer integral $-\sqrt{2}t$, and is characterized by a very low frequency (typically in the microwave region). The electronic Hamiltonian taking into account this mode reads as Equation (4),^[49]

$$h = 2z_0\hat{\rho} - \sqrt{2}(t + \Delta)\hat{\sigma}_x + \frac{\Delta^2}{\varepsilon_c} \quad (4)$$

where Δ is the conformational coordinate measuring the deviation of t from its reference value, and ε_c the corresponding relaxation energy; the

simple hypothesis that a harmonic potential is associated to this mode has been made. Although different in nature, the conformational coordinate can be treated along the same lines as the solvation degree of freedom, that is, in the adiabatic approximation and in the classical limit. The effects of this Peierls-like coupling (increased Stokes shift and additional inhomogeneous broadening) are discussed in the text.

Intermolecular interactions in “dense” systems can be inserted into the model by using the molecular Hamiltonian for each chromophoric entity and adding the interaction term. The form of the Hamiltonian is then Equation (5),^[18,54]

$$H = \sum_i h_i + \frac{1}{2} \sum_i \sum_{j \neq i} V_{ij} \hat{\rho}_i \hat{\rho}_j \quad (5)$$

where V_{ij} measures the interaction between zwitterionic species at positions i and j , and the two summations run over chromophores in the assembly. This Hamiltonian is fairly general: throughout this paper we single out electrostatic forces as the only source of interaction, and choose to assign to each chromophore a fixed length and $+/-e$ charges to the donor/acceptor ends for the zwitterionic basis states. Electrostatic interactions are thus inserted as interactions between charges rather than between dipoles: this allows the length of the chromophores to be taken into account and interactions between spatially close molecules to be described. Since experimental measurements on multichromophore assemblies were made in solution, the interaction terms V_{ij} are screened by the squared refractive index at optical frequencies^[61] ($n^2=2.1$ for CHCl_3). Here dimeric and trimeric multichromophores are considered with symmetries of C_{2v} and C_{3v} , respectively. The length of the chromophore, the interchromophore distance and the angle formed with the main axis of symmetry determine the values of V_{ij} . A few predictions on assemblies made up with different chromophores are also presented.

The Hamiltonian is written on the basis obtained by the direct product of the 2^N electronic states (N =number of chromophores) multiplied the vibrational states. The dimension of the problem is $(2M)^N$, where M is the number of vibrational states introduced for each chromophore.^[18] Eigenvalues and eigenvectors obtained by diagonalization were used to calculate spectra of multimers of series **II**, obtained with $M=8$ (large enough to give converged results). Calculated spectra of multimers of series **I** are not presented, since the large M value needed in this case ($M=18$) leads to a too large a numerical problem.

The values of the first static hyperpolarizability β are obtained through sum-over-states expressions at the experimental frequency ($2\omega=1.3$ eV). In particular, the vector component of the β tensor in the direction of the dipole moment (z) is calculated [Eq. (6)],

$$\beta_z = \frac{1}{3} \sum_i (\beta_{zii} + \beta_{tzi} + \beta_{tzi}) \quad (6)$$

where i runs over Cartesian coordinates (x, y, z). If Kleinman symmetry (valid out of resonance) is imposed,^[62] this expression reduces to $\beta_z = \sum_i \beta_{zii}$. Kleinman symmetry was exploited in the present calculations after checking its validity in the relevant regime. The symmetry of the assemblies is also exploited, so that the following expressions are needed [Eq. (7) and (8)]

$$\beta_z = \beta_{zzz} + \beta_{zyy} \text{ for } C_{2v} + \text{Kleinman symmetry} \quad (7)$$

$$\beta_z = \beta_{zzz} + 2\beta_{zyy} \text{ for } C_{3v} + \text{Kleinman symmetry} \quad (8)$$

$M=8$ molecular vibrations per molecular site were used for calculations in both series.^[63] Throughout this paper β corresponds to the quantity β_z . Moreover, the X convention, as defined in ref. ^[47], is adopted.

Synthesis

General methods: All reactions involving air- or water-sensitive compounds were carried out under argon. Solvents were generally dried and distilled prior to use. Reactions were monitored by TLC on Merck 60 F₂₅₄ aluminum sheets precoated with silica gel. Column chromatography: Merck silica gel Si 60 (40–63 μm , 230–400 mesh), unless otherwise noted.

Melting points were determined on an Electrothermal IA9300 digital melting point instrument. NMR: Bruker ARX 200 (^1H : 200.13 MHz, ^{13}C : 50.32 MHz) or Avance AV 300 (^1H : 300.13 MHz, ^{13}C : 75.48 MHz), in CDCl_3 solutions; ^1H chemical shifts δ are given in ppm relative to TMS as internal standard, J values in Hz and ^{13}C chemical shifts relative to the central peak of CDCl_3 at 77.0 ppm. High-resolution mass spectra were recorded at the Centre Régional de Mesures Physiques de l'Ouest (C.R.M.P.O., Rennes), using a Micromass MS/MS ZABSpec TOF instrument with EBE TOF geometry; liquid secondary ion mass spectrometry (LSIMS) was performed at 8 kV with Cs^+ in *m*-nitrobenzyl alcohol (mNBA).

^{13}C NMR spectra are available as Supporting Information.

4-[Hexyl(2-hydroxyethyl)amino]benzaldehyde (1) was prepared from hexylaniline, analogously to reference [64]; ^1H NMR (200.13 MHz, CDCl_3): δ =9.69 (s, 1H), 7.69 and 6.72 (AA'XX', $J_{\text{A,X}}=9.0$ Hz, 4H), 3.85 (dt, $J=5.8$ Hz, 2H), 3.59 (t, $J=5.8$ Hz, 2H), 3.42 (t, $J=7.8$ Hz, 2H), 1.85 (t, $J=5.8$ Hz, 1H), 1.62 (m, 2H), 1.37–1.29 (m, 6H), 0.90 ppm (t, $J=6.5$ Hz, 3H); ^{13}C NMR (50.32 MHz, CDCl_3): δ =190.2, 152.9, 132.2, 124.8, 111.0, 59.7, 52.7, 51.6, 31.5, 26.7, 26.6, 22.6, 13.9 ppm; HRMS (LSIMS⁺, mNBA): m/z calcd for $\text{C}_{15}\text{H}_{23}\text{NO}_2$ [M^+]: 249.1728; found: 249.1724.

2-[[4-[Hexyl(2-hydroxyethyl)amino]phenylmethylene]propanedinitrile (3). A solution of **1** (0.500 g, 2.0 mmol) and malononitrile (**2**) (0.132 g, 2.0 mmol) in anhydrous ethanol (40 mL) was refluxed for 18 h. After cooling, the solvent was evaporated under reduced pressure and the crude product was purified by column chromatography ($\text{CH}_2\text{Cl}_2/\text{Et}_2\text{O}$ 95/5) to yield **3** (0.490 g; 82%); m.p. 112–113 °C; ^1H NMR (200.13 MHz, CDCl_3): δ =7.80 and 6.72 (AA'XX', $J_{\text{A,X}}=9.3$ Hz, 4H), 7.45 (s, 1H), 3.88 (dt, $J=5.6$ Hz, 2H), 3.62 (t, $J=5.6$ Hz, 2H), 3.46 (t, $J=7.8$ Hz, 2H), 1.64 (m, 2H), 1.55 (t, $J=5.6$ Hz, 1H), 1.33 (m, 6H), 0.91 ppm (t, $J=6.4$ Hz, 3H); ^{13}C NMR (50.32 MHz, CDCl_3): δ =157.7, 153.1, 134.0, 119.1, 116.0, 114.9, 111.7, 71.1, 59.8, 52.6, 51.8, 31.5, 26.8, 26.5, 22.5, 13.9 ppm; HRMS (LSIMS⁺, mNBA): m/z calcd for $\text{C}_{18}\text{H}_{23}\text{N}_3\text{O}$ [M^+]: 297.1841; found: 297.1840.

4-[Hexyl[2-(tetrahydro-2H-pyran-2-yloxy)ethyl]amino]benzaldehyde (4): Pyridinium *p*-toluenesulfonate (PPTS, 0.579 g, 2.3 mmol) was added to a solution of **3** (2.85 g, 11.4 mmol) and 3,4-dihydro-2H-pyran (DHP, 2.10 mL, 23.0 mmol) in anhydrous CH_2Cl_2 (56 mL). The mixture was stirred at 20 °C for 15 h. Water was added, and the organic layer separated and dried (Na_2SO_4). After evaporation of the solvent, the crude product was purified by column chromatography ($\text{CH}_2\text{Cl}_2/\text{AcOEt}$, gradient from 100/0 to 90/10) to yield **4** (3.78 g; 99%); ^1H NMR (200.13 MHz, CDCl_3): δ =9.71 (s, 1H), 7.70 and 6.71 (AA'XX', $J_{\text{A,X}}=9.1$ Hz, 4H), 4.58 (m, 1H), 3.94–3.36 (m, 8H), 1.82–1.42 (m, 8H), 1.33 (m, 6H), 0.90 ppm (t, $J=6.6$ Hz, 3H); ^{13}C NMR (50.32 MHz, CDCl_3): δ =189.8, 152.6, 132.0, 124.8, 110.8, 99.0, 64.5, 62.1, 51.4, 50.5, 31.5, 30.4, 26.7, 26.5, 25.2, 22.5, 19.3, 13.9 ppm; HRMS (LSIMS⁺, mNBA): m/z calcd for $\text{C}_{20}\text{H}_{31}\text{NO}_3$ [M^+]: 333.2304; found: 333.2306.

N-Hexyl-4-[(1E)-2-(4-nitrophenyl)ethenyl]-N-[2-[(tetrahydro-2H-pyran-2-yloxy)ethyl]aminobenzene (6a): NaH (0.188 g, 60% dispersion in mineral oil) was added to a solution of **4** (0.981 g, 2.94 mmol) and diethyl (4-nitrobenzyl)phosphonate (**5**, 0.885 g, 3.24 mmol) in dry THF (25 mL). The mixture was stirred at 20 °C for 16 h. After addition of water (50 mL), the organic layer was separated and dried (Na_2SO_4). After evaporation of the solvent, the crude product was purified by column chromatography (CH_2Cl_2) to yield **6a** (0.794 g; 60%); ^1H NMR (200.13 MHz, CDCl_3): δ =8.17 and 7.55 (AA'XX', $J_{\text{A,X}}=8.8$ Hz, 4H), 7.41 and 6.69 (AA'XX', $J_{\text{A,X}}=8.8$ Hz, 4H), 7.19 (d, $J=16.2$ Hz, 1H), 6.89 (d, $J=16.2$ Hz, 1H), 4.60 (m, 1H), 3.95–3.78 (m, 2H), 3.66–3.43 (m, 4H), 3.37 (t, $J=7.7$ Hz, 2H), 1.88–1.48 (m, 8H), 1.38–1.28 (m, 6H), 0.90 ppm (t, $J=6.5$ Hz, 3H); ^{13}C NMR (50.32 MHz, CDCl_3): δ =148.6, 145.6, 145.0, 133.6, 128.5, 125.9, 124.1, 123.5, 121.0, 111.6, 99.1, 64.8, 62.2, 51.4, 50.5, 31.6, 30.6, 27.0, 26.7, 25.3, 22.6, 19.4, 14.0 ppm; HRMS (LSIMS⁺, mNBA): m/z calcd for $\text{C}_{27}\text{H}_{36}\text{N}_2\text{O}_4$ [M^+]: 452.2675; found: 452.2662.

2-[Hexyl[4-[(1E)-2-(4-nitrophenyl)ethenyl]phenyl]amino]ethanol (6b): 1 M HCl (0.8 mL) was added to a solution of **6a** (0.710 g, 1.57 mmol) in $\text{CH}_2\text{Cl}_2/\text{EtOH}$ (12 mL, 1/1). The mixture was refluxed for 17 h. After cooling, water (24 mL) was added, the mixture was made slightly basic with aqueous NaHCO_3 and extracted with CH_2Cl_2 . The combined organic

layers were dried (Na_2SO_4), the solvent evaporated and the crude product purified by column chromatography ($\text{CH}_2\text{Cl}_2/\text{AcOEt}$, gradient from 100/0 to 97/3) to yield **6b** (0.569 g; 98%); m.p. 111–112°C; $^1\text{H NMR}$ (200.13 MHz, CDCl_3): δ = 8.17 and 7.55 (AA'XX', J_{AX} = 8.8 Hz, 4H), 7.41 and 6.72 (AA'XX', J_{AX} = 9.0 Hz, 4H), 7.19 (d, J = 16.3 Hz, 1H), 6.90 (d, J = 16.3 Hz, 1H), 3.83 (dt, J = 5.9 Hz, 2H), 3.54 (t, J = 5.9 Hz, 2H), 3.37 (t, J = 7.7 Hz, 2H), 1.64 (t, J = 5.9 Hz, 1H), 1.61 (m, 2H), 1.32 (m, 6H), 0.90 ppm (t, J = 6.6 Hz, 3H); $^{13}\text{C NMR}$ (50.32 MHz, CDCl_3): δ = 148.8, 145.8, 144.9, 133.4, 128.5, 126.0, 124.2, 124.1, 121.5, 112.2, 60.1, 52.9, 51.6, 31.6, 26.8, 26.7, 22.6, 14.0 ppm; HRMS (LSIMS⁺, mNBA): m/z calcd for $\text{C}_{22}\text{H}_{28}\text{N}_2\text{O}_3$ [M^+]: 368.2100; found: 368.2100.

2-[Hexyl[4-((1E)-2-(4-nitrophenyl)ethenyl)phenyl]amino]ethyl benzoic ester (I-1): Et_3N (57 μL) and benzoyl chloride (**7**) (28 μL , 0.241 mmol) were added to a solution of **6b** (60 mg, 0.163 mmol) in dry CH_2Cl_2 (0.75 mL, stabilized with amylene) under argon. The mixture was stirred at 20°C for 4 h and then refluxed for 1 h. Water was added and the mixture was extracted with CH_2Cl_2 . The extracts were dried (Na_2SO_4), the solvent evaporated and the crude product purified by column chromatography (CH_2Cl_2) to yield **I-1** (69.5 mg; 90%); $^1\text{H NMR}$ (200.13 MHz, CDCl_3): δ = 8.17 and 7.55 (AA'XX', J_{AX} = 9.0 Hz, 4H), 8.05–8.00 (m, 2H), 7.62–7.53 (m, 1H), 7.49–7.40 (m, 2H), 7.44 and 6.77 (AA'XX', J_{AX} = 8.9 Hz, 4H), 7.20 (d, J = 16.2 Hz, 1H), 6.91 (d, J = 16.2 Hz, 1H), 4.50 (t, J = 6.3 Hz, 2H), 3.76 (t, J = 6.3 Hz, 2H), 3.41 (t, J = 7.7 Hz, 2H), 1.65 (m, 2H), 1.35–1.30 (m, 6H), 0.90 ppm (t, J = 6.4 Hz, 3H); $^{13}\text{C NMR}$ (50.32 MHz, CDCl_3): δ = 166.5, 148.3, 145.8, 144.9, 133.5, 133.1, 129.8, 129.6, 128.6, 128.4, 126.0, 124.2, 124.1, 121.5, 111.9, 61.9, 51.4, 49.3, 31.6, 27.2, 26.7, 22.6, 14.0 ppm; HRMS (LSIMS⁺, mNBA): m/z calcd for $\text{C}_{29}\text{H}_{32}\text{N}_2\text{O}_4$ [M^+]: 472.2362; found: 472.2359.

Bis[2-[hexyl[4-((1E)-2-(4-nitrophenyl)ethenyl)phenyl]amino]ethyl 1,2-benzenedicarboxylic ester (I-2O): Et_3N (51 μL) and **6b** (80 mg, 217 μmol) were added to a solution of phthaloyl chloride (**8a**, 16.7 mg, 82.3 μmol) in dry CH_2Cl_2 (1.0 mL, stabilized with amylene) under argon. The mixture was stirred at 20°C for 4 h and then refluxed for 1 h. Water was added and the mixture was extracted with CH_2Cl_2 . The extracts were dried (Na_2SO_4), the solvent evaporated and the crude product purified by column chromatography (CH_2Cl_2 then $\text{CH}_2\text{Cl}_2/\text{AcOEt}$ 95/5) to yield **I-2O** (60.4 mg; 85%); $^1\text{H NMR}$ (200.13 MHz, CDCl_3): δ = 8.16 and 7.52 (AA'XX', J_{AX} = 8.9 Hz, 8H), 7.68 and 7.55 (AA'XX', 4H), 7.39 and 6.71 (AA'XX', J_{AX} = 8.8 Hz, 8H), 7.15 (d, J = 16.3 Hz, 2H), 6.86 (d, J = 16.3 Hz, 2H), 4.43 (t, J = 6.4 Hz, 4H), 3.70 (t, J = 6.4 Hz, 4H), 3.34 (t, J = 7.6 Hz, 4H), 1.59 (m, 4H), 1.31–1.24 (m, 12H), 0.87 ppm (t, J = 6.6 Hz, 6H); $^{13}\text{C NMR}$ (75.48 MHz, CDCl_3): δ = 167.4, 148.2, 145.8, 144.8, 133.4, 131.7, 131.3, 128.9, 128.6, 126.0, 124.2, 124.1, 121.5, 111.8, 62.4, 51.4, 49.0, 31.6, 27.1, 26.6, 22.6, 14.0 ppm; HRMS (LSIMS⁺, mNBA): m/z calcd for $\text{C}_{52}\text{H}_{58}\text{N}_4\text{O}_8$ [M^+]: 866.4255; found: 866.4261.

Bis[2-[hexyl[4-((1E)-2-(4-nitrophenyl)ethenyl)phenyl]amino]ethyl 1,3-benzenedicarboxylic ester (I-2M): Reaction of isophthaloyl chloride (**8b**) (7.6 mg, 37.4 μmol) with **6b** (40 mg, 108.6 μmol), as described for **I-2O**, afforded **I-2M** (30.7 mg; 95%); $^1\text{H NMR}$ (200.13 MHz, CDCl_3): δ = 8.67 (t, J = 1.7 Hz, 1H), 8.20 (dd, J = 7.5 Hz, 1.7 Hz, 2H), 8.17 and 7.54 (AA'XX', J_{AX} = 8.9 Hz, 8H), 7.53 (t, J = 7.5 Hz, 1H), 7.44 and 6.76 (AA'XX', J_{AX} = 8.8 Hz, 8H), 7.19 (d, J = 16.2 Hz, 2H), 6.90 (d, J = 16.2 Hz, 2H), 4.52 (t, J = 6.4 Hz, 4H), 3.76 (t, J = 6.4 Hz, 4H), 3.40 (t, J = 7.6 Hz, 4H), 1.63 (m, 4H), 1.35–1.27 (m, 12H), 0.89 ppm (t, J = 6.3 Hz, 6H); $^{13}\text{C NMR}$ (50.32 MHz, CDCl_3): δ = 165.6, 148.3, 145.9, 144.9, 134.0, 133.4, 130.8, 130.4, 128.7, 128.6, 126.0, 124.3, 124.1, 121.6, 111.9, 62.3, 51.4, 49.2, 31.7, 27.2, 26.7, 22.6, 14.0 ppm; HRMS (LSIMS⁺, mNBA): m/z calcd for $\text{C}_{52}\text{H}_{58}\text{N}_4\text{O}_8$ [M^+]: 866.4255; found: 866.4245.

Bis[2-[hexyl[4-((1E)-2-(4-nitrophenyl)ethenyl)phenyl]amino]ethyl 1,4-benzenedicarboxylic ester (I-2P): Reaction of terephthaloyl chloride (**8c**, 14.4 mg, 70.9 μmol) with **6b** (80 mg, 217 μmol), as described for **I-2O**, afforded **I-2P** (56.9 mg; 93%); $^1\text{H NMR}$ (200.13 MHz, CDCl_3): δ = 8.18 and 7.56 (AA'XX', J_{AX} = 8.9 Hz, 8H), 8.06 (s, 4H), 7.43 and 6.75 (AA'XX', J_{AX} = 8.9 Hz, 8H), 7.20 (d, J = 16.3 Hz, 2H), 6.91 (d, J = 16.3 Hz, 2H), 4.51 (t, J = 6.1 Hz, 4H), 3.76 (t, J = 6.1 Hz, 4H), 3.39 (t, J = 7.6 Hz, 4H), 1.63 (m, 4H), 1.35–1.25 (m, 12H), 0.89 ppm (t, J = 6.4 Hz, 6H); $^{13}\text{C NMR}$ (50.32 MHz, CDCl_3): δ = 165.6, 148.3, 145.8, 144.9, 133.7, 133.4, 129.6, 128.6, 126.0, 124.3, 124.1, 121.6, 111.9, 62.4, 51.3, 49.2, 31.6,

27.1, 26.7, 22.6, 14.0 ppm; HRMS (LSIMS⁺, mNBA): m/z calcd for $\text{C}_{52}\text{H}_{58}\text{N}_4\text{O}_8$ [M^+]: 866.4255; found: 866.4264.

Tris[2-[hexyl[4-((1E)-2-(4-nitrophenyl)ethenyl)phenyl]amino]ethyl 1,3,5-benzenetricarboxylic ester (I-3): Reaction of 1,3,5-benzenetricarbonyl trichloride (**9**, 9.9 mg, 37.3 μmol) with **6b** (62 mg, 168.3 μmol), as described for **I-2O**, afforded **I-3** (39.0 mg; 83%); $^1\text{H NMR}$ (200.13 MHz, CDCl_3): δ = 8.81 (s, 3H), 8.15 and 7.52 (AA'XX', J_{AX} = 8.8 Hz, 12H), 7.43 and 6.76 (AA'XX', J_{AX} = 8.9 Hz, 12H), 7.16 (d, J = 16.3 Hz, 3H), 6.88 (d, J = 16.3 Hz, 3H), 4.54 (t, J = 6.2 Hz, 6H), 3.76 (t, J = 6.2 Hz, 6H), 3.39 (t, J = 7.4 Hz, 6H), 1.62 (m, 6H), 1.35–1.27 (m, 18H), 0.89 ppm (t, J = 6.4 Hz, 9H); $^{13}\text{C NMR}$ (50.32 MHz, CDCl_3): δ = 164.7, 148.2, 145.8, 144.8, 134.7, 133.3, 131.0, 128.6, 126.0, 124.4, 124.1, 121.6, 111.9, 62.6, 51.3, 49.0, 31.6, 27.1, 26.7, 22.6, 14.0 ppm; HRMS (LSIMS⁺, mNBA): m/z calcd for $\text{C}_{75}\text{H}_{84}\text{N}_6\text{O}_{12}$ [M^+]: 1260.6147; found: 1260.6142.

2-[[4-(2,2-dicyanoethyl)phenyl]hexylamino]ethyl benzoic ester (II-1): Reaction of **3** (57 mg, 0.192 mmol) with benzoyl chloride (**7**, 54 mg, 0.384 mmol), as described for **I-1**, with subsequent purification by column chromatography (heptane/ CH_2Cl_2 60/40 then 40/60), afforded **II-1** (75.6 mg; 98%); m.p. 72–73°C; $^1\text{H NMR}$ (200.13 MHz, CDCl_3): δ = 7.99 (m, 2H), 7.82 and 6.79 (AA'XX', J_{AX} = 9.4 Hz, 4H), 7.63–7.55 (m, 1H), 7.46 (s, 1H), 7.48–7.41 (m, 2H), 4.52 (t, J = 6.3 Hz, 2H), 3.83 (t, J = 6.3 Hz, 2H), 3.48 (t, J = 7.7 Hz, 2H), 1.66 (m, 2H), 1.36–1.29 (m, 6H), 0.90 ppm (m, 3H); $^{13}\text{C NMR}$ (50.32 MHz, CDCl_3): δ = 166.2, 157.8, 152.6, 133.8, 133.2, 129.5, 129.3, 128.4, 119.4, 115.8, 114.7, 111.7, 72.0, 61.3, 51.4, 49.1, 31.4, 26.9, 26.4, 22.4, 13.9 ppm; HRMS (LSIMS⁺, mNBA): m/z calcd for $\text{C}_{25}\text{H}_{27}\text{N}_3\text{O}_2$ [M^+]: 401.2103; found: 401.2093.

Bis[2-[[4-(2,2-dicyanoethyl)phenyl]hexylamino]ethyl 1,2-benzenedicarboxylic ester (II-2O): Reaction of phthaloyl chloride (**8a**, 13.0 mg, 64 μmol) with **3** (58 mg, 195 μmol), as described for **I-2O**, with subsequent purification by column chromatography (heptane/ CH_2Cl_2 30/70), afforded **II-2O** (37.9 mg; 82%); m.p. 76–77°C; $^1\text{H NMR}$ (200.13 MHz, CDCl_3): δ = 7.78 and 6.75 (AA'XX', J_{AX} = 9.1 Hz, 8H), 7.67–7.53 (AA'XX', 4H), 7.44 (s, 2H), 4.46 (t, J = 6.2 Hz, 4H), 3.79 (t, J = 6.2 Hz, 4H), 3.43 (t, J = 7.8 Hz, 4H), 1.62 (m, 4H), 1.35–1.25 (m, 12H), 0.89 ppm (t, J = 6.2 Hz, 6H); $^{13}\text{C NMR}$ (50.32 MHz, CDCl_3): δ = 167.2, 157.8, 152.5, 133.9, 131.5, 131.4, 128.9, 119.6, 115.7, 114.7, 111.8, 72.7, 62.0, 51.5, 49.0, 31.5, 27.0, 26.5, 22.6, 14.0; HRMS (LSIMS⁺, mNBA): m/z calcd for $\text{C}_{44}\text{H}_{48}\text{N}_6\text{O}_4$ [M^+]: 724.3737; found: 724.3728.

Bis[2-[[4-(2,2-dicyanoethyl)phenyl]hexylamino]ethyl 1,3-benzenedicarboxylic ester (II-2M): Reaction of isophthaloyl chloride (**8b**, 13.0 mg, 64 μmol) with **3** (58 mg, 195 μmol), as described for **I-2O**, with subsequent purification by column chromatography (heptane/ CH_2Cl_2 30/70), afforded **II-2M** (43.2 mg; 93%); m.p. 115–116°C; $^1\text{H NMR}$ (200.13 MHz, CDCl_3): δ = 8.57 (s, 1H), 8.15 (d, J = 7.8 Hz, 2H), 7.80 and 6.79 (AA'XX', J_{AX} = 9.1 Hz, 8H), 7.51 (t, J = 7.8 Hz, 1H), 7.44 (s, 2H), 4.53 (t, J = 6.1 Hz, 4H), 3.83 (t, J = 6.1 Hz, 4H), 3.45 (t, J = 7.9 Hz, 4H), 1.65 (m, 4H), 1.31 (m, 12H), 0.88 ppm (t, J = 6.7 Hz, 6H); $^{13}\text{C NMR}$ (50.32 MHz, CDCl_3): δ = 165.3, 157.8, 152.7, 134.0, 133.9, 130.8, 130.0, 128.8, 119.5, 115.7, 114.7, 111.8, 72.3, 61.8, 51.4, 49.0, 31.4, 27.0, 26.5, 22.5, 13.9 ppm; HRMS (LSIMS⁺, mNBA): m/z calcd for $\text{C}_{44}\text{H}_{48}\text{N}_6\text{O}_4$ [M^+]: 724.3737; found: 724.3738.

Bis[2-[[4-(2,2-dicyanoethyl)phenyl]hexylamino]ethyl 1,4-benzenedicarboxylic ester (II-2P): Reaction of terephthaloyl chloride (**8c**, 13.0 mg, 64 μmol) with **3** (58 mg, 195 μmol), as described for **I-2O**, with subsequent purification by column chromatography (heptane/ CH_2Cl_2 30/70), afforded **II-2P** (41.1 mg; 89%); m.p. 155–156°C; $^1\text{H NMR}$ (200.13 MHz, CDCl_3): δ = 8.02 (s, 4H), 7.80 and 6.80 (AA'XX', J_{AX} = 8.9 Hz, 8H), 7.45 (s, 2H), 4.55 (t, J = 5.9 Hz, 4H), 3.85 (t, J = 5.9 Hz, 4H), 3.47 (t, J = 7.5 Hz, 4H), 1.66 (m, 4H), 1.33 (m, 12H), 0.90 ppm (m, 6H); $^{13}\text{C NMR}$ (50.32 MHz, CDCl_3): δ = 165.4, 157.8, 152.7, 133.9, 133.5, 129.6, 119.6, 115.7, 114.7, 111.9, 72.6, 61.9, 51.4, 49.1, 31.5, 27.0, 26.5, 22.5, 13.9 ppm; HRMS (LSIMS⁺, mNBA): m/z calcd for $\text{C}_{44}\text{H}_{48}\text{N}_6\text{O}_4$ [M^+]: 724.3737; found: 724.3732.

Tris[2-[[4-(2,2-dicyanoethyl)phenyl]hexylamino]ethyl 1,3,5-benzenetricarboxylic ester (II-3): Reaction of 1,3,5-benzenetricarbonyl trichloride (**9**, 17.0 mg, 64 μmol) with **3** (87.9 mg, 296 μmol), as described for **I-2O**, with subsequent purification by column chromatography (heptane/ CH_2Cl_2 30/70), afforded **II-3** (23.4 mg; 35%); m.p. 156–157°C; $^1\text{H NMR}$

(200.13 MHz, CDCl_3): $\delta = 8.69$ (s, 3H), 7.80 and 6.81 (AA'XX', $J_{AX} = 9.2$ Hz, 12H), 7.44 (s, 3H), 4.58 (t, $J = 5.9$ Hz, 6H), 3.87 (t, $J = 5.9$ Hz, 6H), 3.47 (t, $J = 7.8$ Hz, 6H), 1.67 (m, 6H), 1.34 (m, 18H), 0.90 ppm (t, $J = 6.5$ Hz, 9H); ^{13}C NMR (50.32 MHz, CDCl_3): $\delta = 164.4$, 157.9, 152.8, 134.8, 134.0, 130.7, 119.7, 115.8, 114.7, 111.8, 72.5, 62.3, 51.2, 48.9, 31.5, 27.0, 26.6, 22.6, 14.0 ppm; HRMS (LSIMS⁺, mNBA): m/z calcd for $\text{C}_{63}\text{H}_{70}\text{N}_9\text{O}_6$ [$M+H$]⁺: 1048.5449; found: 1048.5459.

Acknowledgement

F.T. acknowledges support by a Marie Curie Intra-European Fellowship within the 6th European Community Framework Programme. We acknowledge financial support from DGA (grant N° 00.34.070.00.470.75.653). B.K.G.B. received a postdoctoral fellowship from the French Ministère de l'Éducation Nationale, de l'Enseignement Supérieur et de la Recherche. We are grateful to Prof. I. Ledoux and Prof. J. Zyss for access to EFISHG facilities. Part of the calculations was supported by the "Centre Informatique National de l'Enseignement Supérieur" (CINES-France).

- [1] J. R. Heath, M. A. Ratner, *Phys. Today* **2003**, *56*, 43, and references therein.
- [2] T. C. Lin, S. J. Chung, K. S. Kim, X. P. Wang, G. S. He, J. Swiatkiewicz, H. E. Pudavar, P. N. Prasad in *Polymers for Photonics Applications II* (Ed.: K.-S. Lee), Springer, Berlin, **2003**, pp. 157–193.
- [3] P. N. Prasad, B. A. Reinhardt, *Chem. Mater.* **1990**, *2*, 660–669.
- [4] M. Blanchard-Desce, *C. R. Phys.* **2002**, *3*, 439–448.
- [5] S. R. Marder, B. Kippelen, A. K.-Y. Jen, N. Peyghambarian, *Nature* **1997**, *388*, 845–851.
- [6] Special Issue on Supramolecular Chemistry and Self-Assembly: *Science* **2002**, *295*.
- [7] C. E. Dykstra, *Adv. Chem. Phys.* **2003**, *126*, 1–40.
- [8] S. Di Bella, M. A. Ratner, T. J. Marks, *J. Am. Chem. Soc.* **1992**, *114*, 5842–5849.
- [9] T. Hamada, *J. Chem. Phys.* **1996**, *100*, 8777–8781.
- [10] J. M. Stout, C. E. Dykstra, *J. Am. Chem. Soc.* **1995**, *117*, 5127–5132.
- [11] T. Verbiest, S. Houbrechts, M. Kauranen, K. Clays, A. Persoons, *J. Mater. Chem.* **1997**, *7*, 2175–2189.
- [12] B. Champagne, D. M. Bishop, *Adv. Chem. Phys.* **2003**, *126*, 41–92.
- [13] A. Datta, S. K. Pati, *J. Chem. Phys.* **2003**, *118*, 8420–8427.
- [14] M. Guillaume, E. Botek, B. Champagne, F. Castet, L. Ducasse, *Int. J. Quantum Chem.* **2002**, *90*, 1378–1387.
- [15] M. Drobizhev, Y. Stepanenko, Y. Dzenis, A. Karotki, A. Rebane, P. N. Taylor, H. L. Anderson, *J. Am. Chem. Soc.* **2005**, *127*, 15352–15353.
- [16] W.-H. Lee, H. Lee, J.-A. Kim, J.-H. Choi, M. Cho, S.-J. Jeon, B. R. Cho, *J. Am. Chem. Soc.* **2001**, *123*, 10658–10667.
- [17] M. Barzoukas, M. Blanchard-Desce, *J. Chem. Phys.* **2000**, *113*, 3951–3959.
- [18] F. Terenziani, A. Painelli, *Phys. Rev. B* **2003**, *68*, 165405.
- [19] V. M. Agranovich, M. D. Galanin, *Electronic Excitation Energy Transfer in Condensed Matter*, North-Holland Publishing Company, Amsterdam, **1982**.
- [20] J. Knoester, in *Proceedings of the International School of Physics "Enrico Fermi" 2001, Course CXLIX, Organic Nanostructures: Science and Applications* (Eds.: V. M. Agranovich, G. C. La Rocca), IOS Press, The Netherlands, **2002**, pp. 149–186.
- [21] C. Lambert, W. Gaschler, E. Schmälzlin, K. Meerholz, C. Bräuchle, *J. Chem. Soc. Perkin Trans. 2* **1999**, *2*, 577–587.
- [22] W. Leng, F. Würthner, A. Myers Kelley, *J. Phys. Chem. B* **2004**, *108*, 10284–10294.
- [23] D. Beljonne, W. Wenseleers, E. Zojer, Z. Shuai, H. Vogel, S. J. K. Pond, J. W. Perry, S. R. Marder, J.-L. Brédas, *Adv. Funct. Mater.* **2002**, *12*, 631–641.
- [24] C. Lambert, E. Schmälzlin, K. Meerholz, C. Bräuchle, *Chem. Eur. J.* **1998**, *4*, 512–521.
- [25] A. L. Thompson, K. M. Gaab, J. Xu, C. J. Bardeen, T. J. Martínez, *J. Phys. Chem. A* **2004**, *108*, 671–682.
- [26] S. Tretiak, S. Mukamel, *Chem. Rev.* **2002**, *102*, 3171–3212.
- [27] C. Katan, F. Terenziani, O. Mongin, M. H. V. Werts, L. Porrès, T. Pons, J. Mertz, S. Tretiak, M. Blanchard-Desce, *J. Phys. Chem. A* **2005**, *109*, 3024–3037.
- [28] E. Hendrickx, C. Boutton, K. Clays, A. Persoons, S. van Es, T. Biemans, B. Meijer, *Chem. Phys. Lett.* **1997**, *270*, 241–244.
- [29] H.-J. Deussen, E. Hendrickx, C. Boutton, D. Krog, K. Clays, K. Bechgaard, A. Persoons, T. Bjørnholm, *J. Am. Chem. Soc.* **1996**, *118*, 6841–6852.
- [30] M. Kauranen, T. Verbiest, C. Boutton, M. N. Teerenstra, K. Clays, A. J. Schouten, R. J. M. Nolte, A. Persoons, *Science* **1995**, *270*, 966–969.
- [31] P. J. A. Kenis, O. F. J. Noordman, S. Houbrechts, G. J. van Hummel, S. Karkema, F. C. J. M. van Veggel, K. Clays, J. F. J. Engbersen, A. Persoons, N. F. van Hulst, D. N. Reinhoudt, *J. Am. Chem. Soc.* **1998**, *120*, 7875–7883.
- [32] P. J. A. Kenis, E. G. Kerver, B. H. M. Snellink-Ruël, G. van Hummel, S. Harkema, M. C. Flipse, R. H. Woudenberg, J. F. J. Engbersen, D. N. Reinhoudt, *Eur. J. Org. Chem.* **1998**, 1089–1098.
- [33] T. Verbiest, C. Samyn, C. Boutton, S. Houbrechts, M. Kauranen, A. Persoons, *Adv. Mater.* **1996**, *8*, 756–759.
- [34] E. D. Rekaï, J.-B. Baudin, L. Jullien, I. Ledoux, J. Zyss, M. Blanchard-Desce, *Chem. Eur. J.* **2001**, *7*, 4395–4402.
- [35] E. Kelderman, W. A. J. Starmans, J. P. M. van Duynhoven, W. Verboom, J. F. J. Engbersen, D. N. Reinhoudt, *Chem. Mater.* **1994**, *6*, 412–417.
- [36] S. Yokoyama, T. Nakahama, A. Otomo, S. Mashiko, *J. Am. Chem. Soc.* **2000**, *122*, 3174–3181.
- [37] H. Ma, A. K.-Y. Jen, *Adv. Mater.* **2001**, *13*, 1201–1205.
- [38] E. J. H. Put, K. Clays, A. Persoons, T. Biemans, C. P. M. Luijckx, E. W. Meijer, *Chem. Phys. Lett.* **1996**, *260*, 136–141.
- [39] E. Brouyère, A. Persoons, J.-L. Brédas, *J. Phys. Chem. A* **1997**, *101*, 4142–4148.
- [40] G. P. Bartholomew, G. C. Bazan, *J. Am. Chem. Soc.* **2002**, *124*, 5183–5196.
- [41] G. P. Bartholomew, I. Ledoux, S. Mukamel, G. C. Bazan, J. Zyss, *J. Am. Chem. Soc.* **2002**, *124*, 13480–13485.
- [42] A. Painelli, F. Terenziani, L. Angiolini, T. Benelli, L. Giorgini, *Chem. Eur. J.* **2005**, *11*, 6053–6063.
- [43] J. N. Demas, G. A. Crosby, *J. Phys. Chem.* **1971**, *75*, 991–1024.
- [44] P. Debye, *Polar Molecules*, Dover, New York, **1945**.
- [45] B. F. Levine, C. G. Bethea, *J. Chem. Phys.* **1975**, *63*, 2666–2682.
- [46] J. L. Oudar, D. S. Chemla, *J. Chem. Phys.* **1977**, *66*, 2664–2668.
- [47] A. Willetts, J. E. Rice, D. M. Burland, D. P. Shelton, *J. Chem. Phys.* **1992**, *97*, 7590–7599.
- [48] C. Reichardt, *Chem. Rev.* **1994**, *94*, 2319–2358.
- [49] B. Boldrini, E. Cavalli, A. Painelli, F. Terenziani, *J. Phys. Chem. A* **2002**, *106*, 6286–6294.
- [50] A. Painelli, F. Terenziani, *Chem. Phys. Lett.* **1999**, *312*, 211–220.
- [51] M. M. Tautounji, M. A. Ratner, *J. Phys. Chem. A* **2000**, *104*, 8566–8569.
- [52] Spectra were calculated without taking into account the inhomogeneous broadening effect due to the solvent. This has no influence on the position and integrated intensity of the bands.
- [53] For dimers and trimer of series **II**, dipole moments have not been measured.
- [54] A. Painelli, F. Terenziani, *J. Am. Chem. Soc.* **2003**, *125*, 5624–5625.
- [55] F. Terenziani, A. Painelli, *J. Lumin.* **2004**, *35*, 474–478.
- [56] F. Terenziani, A. Painelli, A. Girlando, R. M. Metzger, *J. Phys. Chem. B* **2004**, *108*, 10743–10750.
- [57] R. S. Mulliken, *J. Am. Chem. Soc.* **1952**, *74*, 811–824.
- [58] A. Painelli, F. Terenziani, *J. Phys. Chem. A* **2000**, *104*, 11041–11048.
- [59] L. Del Freato, F. Terenziani, A. Painelli, *J. Chem. Phys.* **2002**, *116*, 755–761.
- [60] For calculations presented here, eight vibrational states are enough to converge results in series **II**, while at least 18 vibrational states are needed for calculating spectra of series **I**; this is due to the much

- greater vibrational relaxation energy for the chromophore of series **I** than for the chromophore of series **II**.
- [61] G. D. Scholes, *Annu. Rev. Phys. Chem.* **2003**, *54*, 57–87.
- [62] D. A. Kleinman, *Phys. Rev.* **1962**, *126*, 1977–1979.
- [63] While for spectra of products of series **I**, eight vibrational states are not enough, they lead to converged results for ground-state properties.
- [64] M. Mladenova, L. Ventelon, M. Blanchard-Desce, *Tetrahedron Lett.* **1999**, *40*, 6923–6926.

Received: July 28, 2005
Published online: January 23, 2006